eNeuro

Research Article: New Research | Development

Neuron-Specific Gene 2 (NSG2) encodes an AMPA receptor interacting protein that modulates excitatory neurotransmission

Praveen Chander[1], Matthew J. Kennedy[2], Bettina Winckler[3] and Jason P. Weick[1]

[1]*Department of Neurosciences, University of New Mexico-Health Science Center, 145 Reginald Heber Fitz Hall, 915 Camino de Salud NE, Albuquerque, NM 87131, USA*

[2]*Department of Pharmacology, University of Colorado-Denver, 12800 East 19th Ave., Aurora, CO 80045, USA*

[3]*Department of Cell Biology, University of Virginia, 1340 Jefferson Park Avenue, Charlottesville, Virginia, 22908, USA*

https://doi.org/10.1523/ENEURO.0292-18.2018

Received: 25 July 2018

Revised: 13 December 2018

Accepted: 17 December 2018

Published: 4 January 2019

Author contributions: PC designed and performed experiments, analyzed data and wrote the paper. MK and BW contributed critical reagents and wrote the paper. JPW designed and performed experiments, analyzed data, wrote the paper and administered the project.

Conflict of Interest: The authors report no conflict of interest.

Correspondence should be addressed to: Jason P. Weick, PhD, University of New Mexico-HSC, 915 Camino de Salud, NE, Dept. of Neurosciences, Fitz Hall 145, Albuquerque, NM 87131, USA. Phone: 505-272-4410; Fax: 505-272-8082; Email: JPWeick@salud.unm.edu.

Cite as: eNeuro 2018; 10.1523/ENEURO.0292-18.2018

1. Manuscript Title: Neuron-Specific Gene 2 (NSG2) encodes an AMPA receptor interacting protein that modulates excitatory neurotransmission

2. Abbreviated title: NSG2 regulates AMPAR neurotransmission

3. Authors names and affiliations:
Praveen Chander - Department of Neurosciences, University of New Mexico-Health Science Center, 145 Reginald Heber Fitz Hall, 915 Camino de Salud NE, Albuquerque, NM 87131, praveenc@salud.unm.edu

Matthew J. Kennedy, PhD - Department of Pharmacology, University of Colorado-Denver, 12800 East 19th Ave., Aurora, CO 80045, matthew.kennedy@ucdenver.edu

Bettina Winckler, PhD - Department of Cell Biology, University of Virginia, 1340 Jefferson Park Avenue, Charlottesville, Virginia, 22908, bwinckler@virginia.edu

Jason P. Weick, PhD - Department of Neurosciences, University of New Mexico-Health Science Center, 145 Reginald Heber Fitz Hall, 915 Camino de Salud NE, Albuquerque, NM 87131, jpweick@salud.unm.edu

4. Author contributions:
PC designed and performed experiments, analyzed data and wrote the paper. MK and BW contributed critical reagents and wrote the paper. JPW designed and performed experiments, analyzed data, wrote the paper and administered the project.

5. Correspondence should be addressed to:
Jason P. Weick, PhD, University of New Mexico-HSC, 915 Camino de Salud, NE, Dept. of Neurosciences, Fitz Hall 145, Albuquerque, NM 87131, USA. Phone: 505-272-4410; Fax: 505-272-8082; Email: JPWeick@salud.unm.edu

6. Number of figures: 5
7. Number of multimedia: N/A
8. Number of Tables: N/A
9. Number of Extended figures: 8
10. Number of words for Abstract: 185/250
11. Number of words for Significance Statement: 104/120
12. Number of words for Introduction: 644/750
13. Number of words for Discussion: 1224/3000

14. Acknowledgements: We would like to thank the University of New Mexico & Cancer Center Fluorescence Microscopy Shared Resource and Flow cytometry core for assistance with confocal image acquisition and analysis and cell sorting. We also thanks Fernando Valenzuela and Chan Choo Yap for helpful discussions regarding experimental design and methodology.

15. Conflict of Interest: The authors report no conflict of interest.
16. Funding Sources: None

Abstract

Neurons have evolved a number of unique protein-coding genes that regulate trafficking of protein complexes within small organelles throughout dendrites axons. Neuron specific gene 2 (NSG2) encodes for one of the most abundant proteins in the nervous system during perinatal development. NSG2 belongs to a family of small neuronal endosomal proteins but its function has remained uncharacterized to date. Here we show that NSG2 is found in discrete punctae restricted to the somatodendritic arbors of developing mouse and human neurons, and a significant proportion of NSG2 punctae colocalize with postsynaptic HOMER1 and surface-expressed AMPARs at excitatory synapses. Immunoprecipitation revealed that NSG2 physically interacts with both the GluA1 and GluA2 AMPAR subunits in mouse brain. Knockout of NSG2 in mouse hippocampal neurons selectively impaired the frequency of miniature excitatory postsynaptic currents (mEPSCs) and caused alterations in PSD95 expression at postsynaptic densities. In contrast, NSG2 overexpression caused a significant increase in the amplitude of mEPSCs as well as GluA2 surface expression. Thus, NSG2 functions as an AMPAR-binding protein that is required for normal synapse formation and/or maintenance, and has unique functions compared with other NSG family members.

Significance Statement

Due to their morphological and functional complexity, neurons have evolved specialized proteins like those of the neuron-specific gene family (NSG1-3). Important developmental and synaptic functions have been attributed to NSG1/NEEP21 and NSG3/Calcyon while the function of NSG2/HMP19/NVTA2 has remained uncharacterized. Here we show that NSG2 localizes to a large proportion of excitatory synapses, interacts with AMPARs, and modulates their surface expression during synaptogenesis. Alterations of NSG2 expression affected both the amplitude and frequency of excitatory neurotransmission that is not compensated for by other NSG family members. Thus, NSG2 appears critical for excitatory synapse formation and/or maintenance and forced expression can promote increased synaptic efficacy.

Introduction

Neuron-specific gene 2 (NSG2; Neuronal Vesicle Trafficking-Associated 2) belongs to the "neuron-specific gene" family of small, single-pass transmembrane proteins localized to vesicular compartments within neuronal dendrites. The other two NSG family members are NSG1/NEEP21 and NSG3/Calcyon (Muthusamy et al., 2009; Norstrom et al., 2010)lasiecka(Lasiecka et al., 2014), which have been shown to have a number of critical protein trafficking functions primarily involved with neural development and synaptic plasticity. Interestingly, Human NSG2 shares only 50% sequence homology with NSG1 and a 30% sequence homology with Calcyon at the amino acid level (Muthusamy et al., 2009). NSG2 is one of the most highly expressed transcripts and proteins during human neural differentiation and synapse formation (Kang et al., 2011; Miller et al., 2014; Barford et al., 2017; Murillo et al., 2017b). It is expressed widely throughout the brain (Saberan-Djoneidi et al., 1995) with significant overlapping expression but some degree of divergence with NSG1 (Barford et al., 2017). At the cellular level, NSG2 is found extensively localized to the trans-Golgi network as well as in dendritic endosomes, and was recently found to be expressed transiently at the cell surface (Yap et al., 2017). Interestingly, NSG2 also contains a secretogranin III domain as well as an atypical EGF-like motif (Saberan-Djoneidi et al., 1995), making it a good candidate for regulating signaling and exocytosis. However, while much is known about the spatial distribution of NSG2 in dendritic endosomes, its role in neuronal function has remained elusive.

One major function attributed to both NSG1 and NSG3 is the regulated trafficking of the AMPA-type glutamate receptors (AMPARs) at postsynaptic densities (PSDs) during neuronal activity that leads to changes in synaptic efficacy (reviewed in (Yap and Winckler, 2012; Muthusamy et al., 2015). For instance, Calcyon is found in $RAB5^{+}/EEA1^{+}$ early endosomes, interacts with AP2 and AP3, and is critical for clathrin-mediated endocytosis of AMPARs (Xiao et al., 2006; Muthusamy et al., 2012; Muthusamy et al., 2015). Knockout of Calcyon impairs long term depression (LTD)-mediated AMPAR endocytosis, while overexpression reduces GluA1 and

GluA2 surface expression and impairs performance on a fear extinction paradigm (Xiao et al., 2006; Kruusmägi et al., 2007; Davidson et al., 2009a; Vazdarjanova et al., 2011). NSG1, on the other hand, is colocalized to a limited extent with early endosome marker RAB5 and recycling endosome marker RAB11 (Steiner et al., 2002; Yap et al., 2017). Overexpression of the carboxy (C)-terminal tail of NSG1 acts as a dominant negative and prevents recycling of GluA1/2-containing AMPARs following NMDA-mediated internalization (Alberi et al., 2005b; Steiner et al., 2005a). Together these proteins play complementary roles in regulating internalization (Calcyon) and recycling (NSG1) to promote AMPAR sorting between intracellular compartments and the plasma membrane during synaptic plasticity at established synapses. However, the predominant expression of NSG2 during early periods of development (Saberan-Djoneidi et al., 1995; Barford et al., 2017) led us to consider whether it may function during early periods of synaptogenesis. Further, while much is known about AMPAR trafficking at mature synapses, less is known regarding the mechanisms by which AMPARs are trafficked during synaptogenesis.

Here we report that NSG2 is a critical regulator of neuronal AMPAR surface expression in hippocampal cultures during early periods of neuronal development. In agreement with previous reports (Yap et al., 2017), we found NSG2 strongly localized to the trans-Golgi network as well as in a punctate pattern selectively in developing $MAP2^{+}$ dendrites but excluded from axons. In addition, we now uncover that a significant proportion of NSG2 punctae co-localized with synaptic markers including AMPAR subunits. Co-immunoprecipitation and capillary immunoelectrophoresis experiments demonstrated a physical interaction with both GluA1 and GluA2. Overexpression and CRISPR-mediated knockout of NSG2 altered AMPAR surface expression as well as AMPAR-mediated postsynaptic currents. These data are the first to demonstrate a role for NSG2 in the regulation of AMPAR surface expression and implicate NSG2 as a potential partner of AMPARs in regulated endosomal trafficking in developing dendrites.

Materials and Methods

Cell culture, Transfection and Transduction - HEK293T cells and Neuro-2a cells were maintained in DMEM supplemented with 10% fetal bovine serum (FBS) and 1x Penicillin/Streptomycin (Pen/Strep; Thermo Fisher Scientific, Waltham, MA). Cells at 90% confluence were passaged every 3 days using 0.05% Trypsin (Thermo Fisher Scientific). HEK293T cells were transfected using the calcium phosphate method with 10µg plasmid DNA. Neuro-2a cells were transfected using Lipfectamine 3000 (Thermo Fisher Scientific) as per manufacturer's recommendation. Hippocampal pyramidal neurons were derived from P0-P1 C57Bl/6J pups (The Jackson Laboratory, Bar Harbor, ME) of either sex. Briefly, brains were isolated, and the hippocampus was dissected in ice-cold HBSS solution (Sigma, St. Louis, MO) supplemented with 20% FBS and $NaHCO_3$ (4.2mM), HEPES (1mM; Sigma), pH 7.4. Dissected hippocampi were digested for 10 min with 0.25% Trypsin (Thermo Fisher Scientific). Tissue was washed and dissociated using fire polished Pasteur pipettes of decreasing diameter in ice cold HBSS containing DNase (1500 U; Sigma). The cells were pelleted, resuspended in plating media and plated at a density of $4\text{-}5\times10^5$ cells/12-mm coverslip (Electron Microscopy Sciences, Hatfield, PA) coated with poly-Ornithine (0.1mg/ml; Sigma; Cat. #4638) and laminin (5µg/ml; Thermo Fisher Scientific). Cells were allowed to adhere for 20 min before addition of 0.5ml of plating media containing Neurobasal supplemented with 1X B27, 2mM Glutamax, 0.5mg/ml Pen/Strep and 5% FBS (all from Thermo Fisher Scientific) for the first 24h. Serum was eliminated from this media after 24h and again replaced after 48h supplemented with 4µM cytosine 1-β-d-arabinofuranoside (Ara-C; Sigma). Neurons were fed by replacing half the volume of spent media with fresh media without serum or Ara-C every week. All animal procedures were performed in accordance with University of New Mexico-Health Science Center animal care committee's regulations. Neurons on coverslips were transduced with lentivirus (MOI 2 - 3) on day 4 in culture for CRISPR studies or day 7 in culture for NSG2 overexpression studies and assayed at the days indicated in results.

Human pluripotent stem cells (hPSC; line WA09) were maintained in mTesR (Stemcell technologies, Vancouver, Canada) and passaged using 1U/ml Dispase (Stemcell technologies) as per manufacturer's recommendation once the cells reached 80% confluence. hPSC-derived neurons (hPSNs) were differentiated from one six well plate of hPSCs. Briefly, the cells were lifted using Dispase and allowed to grow in suspension in a T75 flask for 4 days in mTeSR. From Day5 to Day20, cells were grown in Neural Induction Media (DMEM/F12; Sigma) supplemented with 1x concentrations of N2, Glutamax and Pen/Strep (Thermo Fisher Scientific) and 2μg/ml heparin (Sigma) to derive neurospheres with 2/3rd volume of media replaced every other day. On Day21, 8 to 10 neurospheres were plated down/12mm glass coverslip in a 24 well dish coated with poly-ornithine and laminin as described above and allowed to attach for a minimum of 4h before feeding with 0.5 ml Neural differentiation media (50:50 mixture of Neurobasal:DMEM/F12 supplemented with 1x concentrations of N2, Glutamax, Pen/Strep and 10ng/ml of cAMP [Sigma], BDNF and GDNF [Peprotech, Rocky Hill. NJ] and 100mM ascorbic acid [Sigma]). Half volume of media was replaced every other day until the assayed days mentioned in the Results section.

Plasmids and Lentivirus production - Episomal vectors encoding mCherry or NSG2-mCherry (NSG2-mC) were generated in house by cloning either mCherry or the open reading frame of human NSG2 (NM_015980.4) in frame with mCherry into the pCS2+ mammalian expression plasmid (kind gift from Bill Bement, Univ. of Wisconsin). The NSG1-GFP plasmid was a kind gift from Bettina Winckler (Univ. of Virginia). The pSIN REP5-GFP-GluA2(R) was purchased from Addgene (Addgene, Cambridge,MA; Cat. # 24005) and the YFP-GluA1 was previously described (Sharma et al., 2006). Lentiviral constructs were generated by cloning either mCherry or NSG2-mC downstream of the Synapsin-1 promoter in the pFCK plasmid (Dittgen et al., 2004). CRISPR/Cas9 guide RNAs (gRNAs) targeting mouse NSG2 (NM_008741.4) were generated using the CRSPR design webtool (https://zlab.bio/guide-design-resources). gRNAs (MsNSG2#1: 5'- GCGTGATGAGAGGGACGGTC-3' and MsNSG2#2: 5'-CGTCCCTCTCATCACGCCCT-3')

were cloned into pL-Crispr.EFS.GFP (Addgene, Cat. # 57818) into the BsmBI site as previously suggested (Heckl et al., 2014). Lentivirus were produced in HEK293T cells using Calcium phosphate transfection of a 15μg total mixture of lentiviral DNA and packaging plasmids psPax2 and pMD2.G (gifts from Didier Trono, Addgene, Cat. # 12260 and Cat. # 12259 respectively) at a ratio of 3:2:1 for lentivirus production. 36-48h post transfection lentivirus containing media was harvested and concentrated using Lenti-X concentrator (Clontech, Mountain view, CA) as per manufacturer's recommendations. Pellets were resuspended in ice cold DMEM, aliquoted, and frozen at −80°C till use.

Cell and Whole brain lysates - HEK293T cells were lysed 48h post transfection by incubating cells for 30min in ice-cold lysis buffer containing (in mM): 50 Tris base, 150 NaCl, 1 EDTA, 1% Triton X-100 and 1x protease inhibitor cocktail (Thermo Fisher Scientific), pH 7.4. Whole brain homogenate was prepared by harvesting mouse brains from P0 pups and subjecting them to a brief ice-cold PBS wash. Brains were then homogenized by sonication (5 x 10sec) in ice cold lysis buffer using a sonic dismembrator (Fisher Scientific, model F60) with output power set at 1. Protein amounts in the supernatant was quantified using the BCA assay (Thermo Fisher Scientific) and was aliquoted and frozen at -80°C until use after cold centrifugation at 10,000 x g for 15 min.

Co-immunoprecipitation - For AMPAR co-immunoprecipitation 2mg total protein was incubated with 4μg of either mouse anti-GluA1 (Clone RH95; Millipore, Billerica, MA), mouse anti-GluA2 (Clone 6C4; Millipore), or control mouse IgG1 (Clone G3A1; Cell Signaling technology, Danvers, MA) antibodies overnight at 4 °C, with gentle rocking. Immune complexes were precipitated for 2h at 4 °C using 20μl protein A/G agarose beads (Santa Cruz Biotechnology). For NSG2-mC co-immunoprecipitation, 1.5mg total protein was incubated with either 50μl anti-RFP mAb-agarose

(MBL intl. corp., Woburn, MA) or RFP-Trap_M (ChromoTek Inc., Hauppauge, NY) according to manufacturer's instructions. Agarose beads from the above reactions were washed and denatured in 50μl 1% SDS and 20μl was loaded on an SDS-PAGE gel for Western Blotting or 2μl of the supernatant was subject to capillary electrophoresis.

Western Blotting and Capillary Electrophoresis - SDS denatured proteins were processed via SDS-PAGE and transferred to FL-PVDF membranes (Li-COR, Lincoln, NE) for traditional immunoblotting. For Western blotting primary antibodies used were rabbit anti-NSG2 (1:500; Abcam, Cambridge, MA), mouse anti-beta-actin (1:5000; Clone AC-15; Thermo Fisher Scientific) and mouse anti-GAPDH (1:500; Clone 6C5; Thermo Fisher Scientific). Secondary antibodies used for detection of primary antibodies were goat anti-mouse 800CW (1:15,000; LiCOR) and goat anti-rabbit 680RD (1:15,000; LiCOR) and blots were scanned using the Odyssey infrared imager and acquired on the Image Studio Lite software suite (Version 3.1, LiCOR). Capillary electrophoresis was performed on the fully automated Wes system (ProteinSimple, San Jose, CA) following the manufacturer's recommendations. Briefly, 0.5μg protein lysate (Input lanes) or 2μl protein (IP lanes) were mixed with 2μl of the 5x Master mix containing SDS and DTT. The samples and protein standard were boiled at 95°C for 5min. The samples were dispensed into microplates containing blocking buffer, primary and secondary antibody and wash buffer in independent wells for sequential processing. The plate was briefly spun and loaded into the instrument for electrophoretic separation of proteins in capillary tubes containing a 12-250kDa separation matrix. The chemiluminescence based electrophoretogram was auto generated and digitally-rendered bands shown in Figure 3 were generated from the chemiluminescent peaks using the Compass software (ProteinSimple). For the Wes, primary antibodies were rabbit anti-NSG2 (1:300), mouse anti-GluA1 (1:100) and mouse anti-GluA2 (1:50). HRP-conjugated

secondary anti-mouse and anti-rabbit antibodies were used at the predefined concentrations provided by the manufacturer.

T7 Endonuclease I assay – Neuro-2a cells were transfected with either the control or CRISPR NSG2 KO gRNA plasmids and allowed to express the constructs for 48-60h. The cells were then harvested and a purified GFP^+ cells population was obtained by flow cytometry. The genomic DNA from the GFP^+ cell population was extracted using a commercially available kit (Zymo Research, Irvine, CA). 100μg of genomic DNA was used as a template for PCR amplification of a fragment surrounding the putative gRNA cleavage site using the following primer pair: Fwd 5'-tccccggacaatgggaatcatg-3' and Rev 5'-gtggctggaagaatgaaaggat-3'. Amplicons were then subjected to a single cycle of denaturation and renaturation to generate heteroduplex molecules containing mismatches which could be recognized and cleaved using the T7 endonuclease I enzyme (New England Biolabs, Ipswich, MA). The products of the reaction were resolved on a 2% agarose gel containing 1x gel red stain (Biotium, Fremont, CA) and imaged on a gel documentation system (Biorad, Hercules, CA). The relative band intensities of the cut fragments to the uncut fragment were used to calculate the gRNA-mediated cleavage efficiency.

Immunocytochemistry – Neurons on coverslips were fixed with 4% paraformaldehyde/4% sucrose for 15min, rinsed 3 times for 5min in phosphate-buffered saline (PBS; Sigma), and permeabilized using 0.2% Triton for 10min (except when staining for surface GluA1 and GluA2). Cells were blocked with 10% donkey serum in PBS for 1h, followed by an overnight incubation of primary antibody in 5% donkey serum at 4°C. Primary antibodies consisted of rabbit anti-NSG2 (1:500; Abcam), goat anti-NSG1 (1:400; Everest Biotech, Oxford, UK), mouse anti-GFAP (1:1000; Neuromab, Davis, CA), chicken anti-β_{III}-tubulin (1:500; Millipore), rabbit anti-Homer1 (1:1000; Synaptic Systems, GmbH, Goettingen, Germany), guinea pig anti-Homer1 (1:200; Synaptic

Systems), mouse anti-Synapsin-1 (1:2000; Synaptic Systems), chicken anti-MAP2 (1:5000; Biolegend, San Diego, CA), mouse anti-SMI312 (1:1000; Biolegend), mouse anti-PSD95 (Clone 7E3, 1:100; Thermo Fisher Scientific), and antibodies targeting the amino(N)-terminus of GluA1 and GluA2 (1:100) (see "coimmunoprecipitation" section). Following primary antibody incubation cells were washed thrice with PBS and incubated for 1h with secondary antibody in 5% donkey serum. Conjugated secondary antibodies used were: DyLight 488, 550 and 647 (1:1000; Thermo Fisher Scientific), donkey anti-guinea pig CF555 and goat anti-chicken CF647 (both at 1:500; Sigma). Cells were washed with PBS and then in some cases treated with DAPI (1:10,000 in PBS; Thermo Fisher Scientific), followed by 3 washes with 1X PBS, and mounted on superfrost slides on Fluoromount-G as an anti-quenching reagent (Southern Biotech, Birmingham, AL). In our hands the GluA1 antibody described above did not yield much success with hPSNs. Therefore, we carried out live staining for surface GluA1 on hPSNs with a custom developed rabbit anti-GluA1 targeting the extracellular epitope of GluA1 (1:200; a kind gift from Dr. Matthew Kennedy, UC Denver). The cells were incubated live with the antibody for 15min before three brief PBS washes and fixation with 4% PFA. The post fixation treatments and secondary antibody incubations were same as described above.

Confocal Imaging and Analysis - Confocal z-stacks were acquired on the Zeiss LSM800 airyscan confocal microscope using the 63x/1.40NA Oil objective. Sequential frame acquisition was set to acquire an average of 10 planes per stack at 16bit and a minimum of 1024x1024 resolution. Channel gain settings were optimally adjusted to minimize saturation of punctae and were maintained across experimental groups. Unmodified images were utilized for all analyses and linear scaling was applied on images only for presentation purposes using Zen Black 2.3 (https://www.zeiss.com/microscopy/us/downloads/zen.html). Fluorescent signal colocalization on the single planes from a stack and quantification of punctae number was performed using the colocalization plugin for ImageJ ComDet version 0.3.4 (https://github.com/ekatrukha/ComDet) as

303 previously described (Esteves da Silva et al., 2015). Punctae integrated fluorescence intensity
304 over area measurements were performed with ImageJ 1.48v (https://imagej.nih.gov/ij/). For each
305 experimental group an average of greater than 200μm dendrite was quantified for 8 to 10 images
306 per experiment and repeated for a total of three biological replicates.
307
308 **Electrophysiology -** Whole cell patch-clamp recordings were performed a previously described
309 (Weick et al., 2013) with minor modifications. The extracellular solution was a modified Hanks'
310 balanced salt solution (HBSS) that contained (in mM): 140 NaCl, 3 KCl, 2 $CaCl_2$, 1 $MgCl_2$, 15
311 HEPES, and 23 glucose, pH 7.4, 300 mOsm. Recording pipettes with resistances of 3 to 5 MΩ
312 were filled with an intracellular recording solution containing the following (in mM): 121 K-
313 gluconate, 20 KCl, 2 $MgCl_2$, 10 EGTA, 10 HEPES acid, 2 Mg^{2+}-ATP, 0.2 Na^{+}-GTP, pH 7.2,
314 290 mOsm. Pharmacological antagonists picrotoxin (50μM; Tocris, Bristol, UK), TTX (1μM;
315 Tocris), and AP5 (25μM; Sigma) were bath applied in the external solution. Each experiment
316 consisted of 10 to 13 cells per group and experiments were repeated three times on different
317 cultures at the same time points indicated in the results. Neurons were visualized using an
318 Olympus Optical BX51WI microscope (Olympus Corp., Tokyo, Japan) with differential
319 interference contrast optics at 40x. Recordings were obtained using a MultiClamp 700B amplifier
320 (Molecular Devices, Sunnyvale, CA), filtered at 4 kHz and sampled at 100 kHz using a Digidata
321 1322A analog-to-digital converter (Molecular Devices). Whole-cell capacitance was fully
322 compensated but series resistance was not compensated. Access resistance was monitored
323 before and after recordings, and cells with resistances greater than 20 MΩ at either point were
324 discarded from analyses. Miniature excitatory postsynaptic currents (mEPSCs) were measured
325 using a holding potential of -70mV while outward potassium currents were elicited by a voltage-
326 step protocol from -50mV to +50mV, and all recordings were performed at 32°C. Step protocols
327 were used to verify the lack of inward sodium current in all cells used for subsequent analysis.
328 Data were stored on a computer hard disk and postsynaptic currents (PSCs) were analyzed using

MiniAnalysis software (Synaptosoft, Fort Lee, NJ) while potassium currents were analyzed using Clampfit v. 10.0 (Molecular devices). The cells utilized for mEPSC recordings for NSG2 knockout (control GFP and CRISPR NSG2 KO) were injected with Lucifer yellow (10mM; Thermo Fisher Scientific) included in the internal solution. After recordings cells were immediately fixed and stained for NSG2 as described above (see methods; immunocytochemistry). Only cells showing a lack of NSG2 (indicating NSG2 KO) were included for subsequent analysis.

Statistical Analyses - Student's *t*-tests were used to determine whether mean differences between groups (e.g., control mCherry vs. NSG2-mC) were significant and were considered significant a priori if $p < 0.05$. The number of samples used for statistical analyses (*n*) refers to the number of cells assayed per group accumulated from three independent biological replicates for all imaging-based assays and electrophysiology experiments. For analysis of synaptic and NSG2 punctae, n's are still reported by the criteria above but at least 1500 total punctae were included across cells/replicates. Data are reported as Mean ± Standard Error of Mean (S.E.M).

Data Availability - Data generated and analyzed in this study are available from the corresponding author upon request.

Results

NSG2 is localized to postsynaptic densities of excitatory synapses

NSG2 is one of the most highly upregulated and abundant mRNAs during early neuronal development across multiple species, including human (Kang et al., 2011; Miller et al., 2014; Barford et al., 2017; Murillo et al., 2017a). To determine whether NSG2 *protein* was similarly upregulated, we first used differentiation of cortical neurons derived from human pluripotent stem cells (hPSCs) and assayed for NSG2 using an antibody previously shown to detect the rodent

protein (Barford et al., 2017). Robust NSG2 expression was observed in 98% of the β_{III}-Tubulin$^+$ neurons analyzed (n=151/154 neurons from 5 independent experiments) at days 30 and 50 in culture (Figure 1-1, A-B). These timepoints correspond to periods prior to and following the formation of functional synapses in hPSC-derived neurons (hPSNs), respectively. NSG2 was not found in neuroepithelial cells at Day30 that were PAX6$^+$/MAP2$^-$ (Figure 1-1, C), suggesting its upregulation following the final mitotic division. Similarly, NSG2 was detected by 4 days *in vitro* (DIV4) in cultured mouse hippocampal neurons (Figure 1A), an early timepoint prior to the creation of functional synapses (Grabrucker et al., 2009). NSG2 remained robustly expressed in all hippocampal neurons examined (n=391/391; from six independent cultures) at all time points assayed up to DIV30 (Figure 1-2). Similar to previous reports, NSG2 was found robustly aggregated in perinuclear regions consistent with localization to the Golgi apparatus (Saberan-Djoneidi et al., 1995) as well as in distinct punctae throughout β_{III}-tubulin$^+$ neurites (Figure 1A and yellow box magnified in Figure 1B, blue; arrows; Figure 1-1). At DIV4, NSG2 was absent from GFAP$^+$ astrocytes in regions that did not have overlapping β_{III}-tubulin$^+$ neurites (Figure 1A and yellow box magnified in Figure 1B, cyan; arrowheads). This was also evident in cultures of human neurons and glia at Day50 (Figure 1-3, A), supporting the neuron-specific nature of NSG2 across species. At DIV14 in mouse neurons, the number of NSG2 punctae were dramatically increased as neuronal arbors became more elaborate (Figure 1C). At this time point, NSG2 punctae were restricted to the somatodendritic compartment as MAP2$^+$ dendrites showed robust staining (Figure 1C and yellow box magnified in Figure 1D, Figure 1-3, B, blue; arrows) whereas SMI-312$^+$ axons were devoid of NSG2 (Figure 1C and yellow box magnified in 1D, Figure 1-3, B, cyan; arrowheads). Together, these data support the neuron-specific nature of NSG2 and show its punctate localization restricted to somatodendritic arbors of human and mouse neurons.

In contrast to previous reports suggesting that NSG2 protein is nearly absent in brain following early postnatal development (Saberan-Djoneidi et al., 1995), Barford et al. recently showed that expression of NSG2 was maintained in cortex up to the period of adolescence (P16) but was

absent from cerebellum in adults (P60; (Barford et al., 2017)). Due to sequence homology between NSG family members we determined whether the antibody used for immunostaining was specific for NSG2. Western blot analysis was used to validate the specificity of the NSG2 antibody, which revealed a band of approximately 47kDa in lysates taken from HEK293T cells overexpressing NSG2 (19kDa) linked to the mCherry (28kDa) fluorophore (NSG2-mC; Figure 1E, upper panel, middle lane). However, no bands were detected in lysates taken from HEK293T cells overexpressing NSG1 (21kDa) linked to GFP (27kDa; Figure 1E, upper panel, right lane) or untransfected HEK293T cell lysates (Figure 1E, upper panel, left lane). β-actin served as a loading control (Figure 1E, lower panel). Further, to determine the expression profile of endogenous NSG2 protein over time we performed western blot of mouse whole brain lysates. We found that while NSG2 has its greatest expression during the perinatal period and is gradually downregulated thereafter, it continues to be expressed even in adult animals (P60; Figure 1F) consistent with recent studies (Barford et al., 2017).

Due to the punctate nature of NSG2 expression in dendrites, we determined whether NSG2 localized to synapses. In DIV14-16 hippocampal neurons a portion of endogenous NSG2 (endo-NSG2) punctae was independent of both presynaptic Synapsin-1 (SYN1) and post-synaptic HOMER1 (Figure 1G, arrow), whereas strong synaptic localization was observed for a subset of endo-NSG2 punctae (Figure 1G, left panels, arrowheads). Quantification of colocalization showed that approximately 30% of HOMER1 punctae colocalized with NSG2. By comparison, NSG2 punctae were frequently found adjacent to, but not colocalized with SYN1 punctae (Figure 1G, left arrowhead). In fact, some endo-NSG2 punctae were found colocalized with HOMER1 that were not adjacent to SYN1 punctae (Figure 1G, left panels, far right arrowhead). Similar results were found with overexpressed NSG2-mC (Figure 1G, right panels), indicating this construct behaves similarly to the endo-NSG2 protein. Interestingly, the percentage of HOMER1 punctae that colocalized with NSG2-mC was significantly increased compared to that for endo-NSG2 (Figure 1H; endo-NSG2: 29.2% ± 2.5; NSG2-mC: 37.0% ± 2.0; *p = 0.024). This happened

406 despite the fact that the total densities of HOMER1 punctae for control and NSG2-mC were not
407 significantly different (mCherry: 126 ± 7 punctae/100µm; NSG2-mC: 133 ± 10 punctae/100µm; p
408 = 0.6). Thus, the increased colocalization between NSG2-mC and HOMER1 is likely a result of
409 NSG2-mC entering HOMER1^{+} synapses that are not occupied by endo-NSG2. Taken together
410 these data suggest that NSG2 is present in a subset of excitatory synapses, and is likely restricted
411 to the postsynaptic density rather than presynaptic terminals. Furthermore, overexpressed NSG2-
412 mC was not sufficient to drive formation of new HOMER1^{+} PSDs, but was able to enter new sites
413 where endo-NSG2 was likely absent.
414
415 **NSG2 interacts with AMPAR subunits GluA1 and GluA2**
416 To determine whether NSG2 colocalizes with functional AMPAR-containing synapses, we
417 used surface labeling with antibodies directed toward the extracellular N-termini of the GluA1 and
418 GluA2 subunits. Figure 2A-B shows representative confocal images of neurons (left panels) as
419 well as individual neurites (right panels) from boxed regions. Results for both GluA1 and GluA2
420 revealed robust colocalization with individual NSG2 punctae (Figure 2A-B, right panel
421 arrowheads). Pooled data revealed that approximately 40% of NSG2 punctae colocalized with
422 either the GluA1 (Figure 2A, C; NSG2/GluA1: 40.1% ± 1.6) or GluA2 subunits (Figure 2B, D;
423 NSG2/GluA2: 41.0% ± 1.5). Reciprocally, over 45% of GluA1 and GluA2 surface labeled punctae
424 colocalized with NSG2, suggesting that nearly half of all AMPAR-containing postsynaptic
425 densities contained NSG2 protein at DIV15 (Figure 2C-D; GluA1/NSG2: 46.2% ± 1.2;
426 GluA2/NSG2: 48.0% ± 0.9). It is noteworthy that the percent of colocalization between AMPAR
427 subunits and NSG2 was slightly greater than that of HOMER1/NSG2, indicating that NSG2 is
428 somewhat selective for AMPAR-containing PSDs. We additionally verified that overexpressed
429 NSG2-mC colocalized with human GluA1 subunits in hPSNs at Day50. While these data revealed
430 significant colocalization of NSG2 with surface GluA1 in hPSNs (Figure 2-1), the inconsistent
431 maturational state of individual hPSNs (Johnson et al., 2007) makes characterization of NSG2

function more difficult. Thus, all future experiments were conducted on cultured mouse hippocampal neurons.

We next determined whether NSG2 physically associates with AMPAR subunits GluA1 and GluA2. We first performed co-immunoprecipitation (Co-IP) from HEK293T cells co-expressing the fusion proteins NSG2-mC (approx. 45kDa) and either YFP-GluA1 or GFP-GluA2 (approx. 128kDa and 125kDa, respectively). Using an anti-mCherry monoclonal antibody we immunoprecipitated NSG2-mC and probed for YFP-GluA1 and GFP-GluA2 using antibodies specific for each subunit. Figure 3A shows data from a capillary immunoelectrophoresis that demonstrates NSG2-mC was able to Co-IP both GluA1 and GluA2 independently (lanes marked IP: mCherry) when the two proteins were co-expressed in HEK293T cells. An IgG control antibody did not IP either NSG2 or AMPAR subunits demonstrating the specificity of the reaction (Figure 3A, IP: IgG); the heavy chain of the control mouse IgG antibody is detected by the anti-mouse secondary antibody used to detect GluA1 and 2. To further validate our findings we used the traditional Co-IP/SDS-PAGE to probe for a NSG2-mC and GluA2 interaction (Figure 3-1, middle lane). In this case, 24h incubation of lysates taken from HEK293T cells that expressed either protein separately showed significantly reduced Co-IP, suggesting that their co-expression in a cellular context may be necessary to drive NSG2-GluA2 interactions (Figure 3-1, right lane). We also performed the complementary experiment to verify the interaction of overexpressed proteins. Immunoprecipitation of either GluA1 or GluA2 using antibodies previously described (Schwenk et al., 2014) could Co-IP both overexpressed NSG2 (Figure 3B, arrow) as well as endogenous NSG2 (Figure 3C, arrow). In this case we used whole cell lysates from HEK293T cells co-expressing either GFP-GluA2 or YFP-GluA1 with unlabeled NSG2 (approx. 19kDa) to demonstrate that non-specific interactions between the fluorophores played no role in the interactions. In Figure 3B, the lanes marked IP: GluA1 and IP: GluA2 indicate that both GluA1 and GluA2 were able to Co-IP NSG2 (lower band, arrow). Finally, we asked whether the interaction between NSG2 and GluA1 and GluA2 subunits of AMPARs occurs *in vivo*. Utilizing

458 whole brain protein lysates from P0 mouse we found that immunoprecipitation of either GluA1 or
459 GluA2 AMPAR subunits pulled down endo-NSG2 (Figure 3C; lanes marked IP: GluA1 and IP:
460 GluA2). Non-specific mouse IgG antibody did not pull down either AMPARs or NSG2 (Fig 3A, 3B,
461 3C; lanes marked IP: IgG). Heavy and light chains of control IgG are present similar to heavy
462 chain in Figures 3A-B; lowest bands in "IP: IgG" group are likely non-specific as they appear in all
463 groups and are of lower molecular weight compared to NSG2.
464
465 **NSG2 expression affects AMPAR currents**
466 Since NSG2 colocalizes with and is found in a complex with AMPAR subunits GluA1 and
467 GluA2, we next asked if manipulating NSG2 protein levels would alter AMPAR surface expression
468 as well as excitatory synaptic transmission. Two CRISPR/Cas9 guide RNAs (gRNAs) were
469 designed using the MIT CRISPR design tool to target the mouse NSG2 locus. A T7 endonuclease
470 cleavage assay determined that both gRNA#1 and gRNA#2 created indels in the NSG2 locus in
471 mouse Neuro-2a neuroblastoma cells. However, the efficiency (Figure 4-3C) of gRNA#2 was
472 significantly greater than gRNA#1, so this one was used for all experiments in primary
473 hippocampal neurons. Transduction of control CRISPR virus and NSG2 gRNA was performed at
474 DIV4 and neurons were analyzed at DIV16-18. Figure 4A (upper panels) shows robust NSG2
475 punctae (arrowheads) in neurons transduced with control CRISPR lentivirus. In contrast, neurons
476 transduced with the CRISPR gRNA targeting NSG2 resulted in a complete knockout of NSG2
477 (Figure 4A, lower panels; NSG2 KO; arrow). Note that no effect on NSG2 expression was
478 observed in adjacent, non-transduced neurons (Figure 4A, lower panels, arrowhead).
479 Interestingly, the quantification of NSG2 KO in neurons transduced with NSG2 CRISPR virus
480 revealed that approximately 70% of neurons (n=38/55, from 3 independent cultures) had a
481 complete KO. To confirm specificity of CRISPR targeting, we analyzed NSG1 expression in
482 neurons that expressed NSG2 gRNA and showed complete KO of NSG2 protein. These neurons
483 showed no significant difference in the density of NSG1 punctae compared to neurons expressing

484 control CRISPR constructs (Figure 4-3B; control: 346.3 ± 137.75 punctae/100μm; NSG2 KO:
485 354.3 ± 134.26 punctae/100μm; p = 0.97). To determine the effect of NSG2 KO on synaptic
486 transmission we performed whole-cell patch clamp recordings on GFP$^+$ neurons that received the
487 CRISPR-NSG2 KO virus. To eliminate possible contamination from the small proportion of
488 neurons that did not show NSG2 KO, we used Lucifer Yellow injections followed by post-hoc
489 analysis of KO efficiency by immunocytochemistry to correlate NSG2 levels with physiological
490 recording data (Figure 4-1; only cells with undetectable NSG2 signal were used for analysis).
491 Figure 4B shows representative traces of voltage-clamp recordings from neurons expressing
492 control CRISPR (black) or NSG2 KO CRISPR virus (green). Compared to control neurons, NSG2
493 KO neurons showed a significant decrease in the frequency of miniature excitatory postsynaptic
494 currents (mEPSCs), with no change in amplitude (Figure 4B-C; Frequency; control: 12.41 ± 2.31
495 Hz; NSG2 KO: 4.07 ± 0.68 Hz; **p = 0.001; Amplitude; control: 16.71 ± 4.10 pA; NSG2 KO: 15.84
496 ± 4.47 pA; p = 0.34). These effects were specific to synaptic currents as voltage-gated potassium
497 currents remained unchanged (Figure 4-2). To probe the mechanism of how NSG2 might affect
498 mEPSCs, we performed immunocytochemical labeling of multiple synaptic proteins. NSG2 KO
499 did not affect the density of presynaptic SYN1$^+$ nor postsynaptic PSD95$^+$ punctae along neurites
500 (Figure 4D; SYN1; control: 93 ± 8 punctae/100μm; NSG2 KO: 79 ± 7 punctae/100μm; p = 0.46;
501 PSD95; control: 97 ± 7 punctae/100μm; NSG2 KO: 80 ± 9 punctae/100μm; p = 0.18). Interestingly,
502 the fluorescence intensity of PSD95$^+$ punctae was significantly decreased in NSG2 KO neurons
503 compared to controls (Figure 4E; control: 3.70 ± 0.45 A.U.; NSG2 KO: 2.57 ± 0.28 A.U.; *p =
504 0.04). This occurred without a corresponding change in the density of GluA1- and GluA2-
505 containing punctae along neurites (Figure 4F; surface GluA1$^+$; control: 86 ± 8 punctae/100μm;
506 NSG2 KO: 83 ± 12 punctae/100μm; p = 0.86 and surface GluA2$^+$; control: 94 ± 7 punctae/100μm;
507 NSG2 KO: 74 ± 12 punctae/100μm; p = 0.18). Together, these data indicate that the reduction in

mEPSC frequency due to loss of NSG2 may be caused by a relatively subtle effect on postsynaptic scaffolding rather than a failure of AMPAR exocytosis.

To test whether NSG2 can augment postsynaptic targeting of AMPARs we used overexpression of NSG2-mC, which shows nearly identical synaptic targeting as endo-NSG2 (Figure 1D). Figure 5A shows representative traces of voltage-clamp recordings from neurons overexpressing mCherry (black) alone or NSG2-mC (red). Pooled data revealed that neurons expressing NSG2-mC showed a significant increase in mEPSC amplitude compared to those expressing mCherry alone (Figure 5A, B; mCherry: 21.61 ± 1.43 pA; NSG2-mC: 30.22 ± 3.07 pA; **p = 0.01). In contrast to NSG2 KO, no significant difference was observed for mEPSC frequency upon NSG2 overexpression (Figure 5B; mCherry: 12.88 ± 2.91 Hz; NSG-mC: 17.66 ± 4.12 Hz; p = 0.35). Immunocytochemical analyses revealed that the intensity of GluA1 and GluA2 staining showed a trend toward an increase but that did not reach significance (Figure 5C, E; Fluorescence Intensity of GluA1; mCherry: 1.00 ± 0.38 A.U.; NSG2-mC: 1.63 ± 0.54 A.U.; p = 0.36 and GluA2; mCherry: 1.00 ± 0.11 A.U.; NSG2-mC: 1.32 ± 0.21 A.U.; p = 0.19). Interestingly, while the number of surface GluA1$^+$ punctae remained unchanged (Figure 5C; mCherry: 92 ± 10 punctae/100µm; NSG2-mC: 97 ± 8 punctae/100µm; p = 0.58), the number of GluA2$^+$ punctae was significantly increased upon NSG2-mC overexpression (Figure 5E; mCherry: 94 ± 6 punctae/100µm; NSG2-mC: 123 ± 10 punctae/100µm; *p = 0.02). These data suggest that NSG2 is sufficient to drive increased surface expression of AMPARs into existing functional synapses, and potentially to a small proportion of previously silent synapses.

DISCUSSION

While critical roles in endosomal trafficking and synaptic plasticity have been established for NSG1 and NSG3, no functional role for NSG2 has previously been demonstrated. Here we present evidence that NSG2 is a novel modulator of excitatory synaptic function. We found NSG2 displays a punctate pattern of expression that is restricted from axons but found robustly

throughout somatodendritic arbors. Approximately forty percent of all postsynaptic densities that contained surface expressed AMPAR subunits also displayed colocalized NSG2 punctae. Reciprocal immunoprecipitation assays revealed that NSG2 interacts with both GluA1 and GluA2 AMPAR subunits *in vitro* and *in vivo*. CRISPR/Cas9-mediated knockout of NSG2 in primary hippocampal neurons resulted in a significantly reduced frequency of AMPAR-mediated mEPSCs, in the absence of a reduction in total surface expressed AMPAR levels. Surprisingly, overexpression of NSG2 caused a significant increase in the amplitude of AMPAR-mediated mEPSCs that was coincident with increased surface expression of the AMPAR subunit GluA2, but did not affect frequency as in the knock out condition. Together, these data suggest NSG2 is a novel player in excitatory postsynaptic function potentially via trafficking of AMPAR and/or associated cargo proteins (see below).

While it remains unclear as to how NSG2 modulates excitatory synaptic function specifically, the preponderance of evidence points to the regulation of AMPAR surface expression via secretory trafficking. This is supported by our current findings in conjunction with a number of findings for other NSG family members. For instance, NSG3 facilitates clathrin-mediated *endocytosis* of AMPARs during agonist stimulated activity that causes synaptic depression (Xiao et al., 2006; Davidson et al., 2009a). Overexpression of NSG3 was shown to cause internalization of GluA1 and GluA2, decreasing surface expression levels of AMPARs. Furthermore, chronic upregulation of NSG3 in a transgenic mice was shown to impair executive cognitive function (Xiao et al., 2006; Kruusmägi et al., 2007; Davidson et al., 2009a; Vazdarjanova et al., 2011), likely via alterations in AMPAR trafficking and altered long-term depression like processes (Myers et al., 2006; Kim et al., 2007). In contrast, NSG1 has been shown to regulate the rate of AMPAR receptor recycling within the post-synaptic density (Steiner et al., 2005b; Utvik et al., 2009). While no studies report the functional consequences of full-length NSG1 overexpression, inhibition of NSG1 function via a dominant negative peptide prevented constitutive recycling of GluA1/2-containing AMPARs following NMDA-mediated internalization (Alberi et al., 2005b; Steiner et al.,

2005a). Similarly, antisense-mediated suppression of NSG1 function severely impaired the amplitude of evoked potentials in organotypic hippocampal slices (Alberi et al., 2005a). However, it is not clear whether the observed effect on amplitude was a consequence of a reduction in the number of AMPARs within individual synapses, or a reduction in the number of synapses that contained AMPARs. For example, Levy et al., demonstrate that the effect of changing levels of the MAGUK family of scaffolding proteins, specifically knockdown of PSD95 causes a reduction in AMPAR mEPSC frequency in dissociated hippocampal neurons by increasing the number of silent synapses, however without affecting mEPSC amplitudes (Levy et al., 2015). Thus, one explanation for our observations could be that in NSG2 KO neurons, a subset of synapses that would have contained NSG2 showed reduced or altered AMPAR localization that our methods were not sensitive enough to detect via immunocytochemistry. In this case, these synapses demonstrated increased failure rates or sub-threshold events which resulted in a decrease in mEPSC frequency. However, the absence of an effect on AMPAR surface expression suggests either subtle changes in AMPAR localization or an alternate mechanism. We cannot rule out a role of NSG2 on presynaptic function, although manipulation of NSG1 and NSG3 does not alter presynaptic release (Alberi et al., 2005a; Davidson et al., 2009b), and NSG2 is solely found in the post-synaptic density (Figures 1 and 2). (Alberi et al., 2005b; Steiner et al., 2005a)While future studies are needed to elucidate the mechanistic details of how NSG2 is involved in regulating AMPAR trafficking, our data support a complementary role of NSG2 with that other NSG family members.

One mechanism likely involves secretion of AMPARs via Post-Golgi endosomal vesicles that may contain individual or combinations of NSG family members depending on function. For instance, Yap and colleagues recently demonstrated that both NSG1 and NSG2 puncta in dendrites show approximately sixty percent overlapping expression with the remaining forty percent not co-localized. Interestingly, a significant proportion of overlap was found in $Rab7^{+}$ late endosomes traveling in a retrograde fashion which the authors conclude were likely destined for

586 degradation. Smaller proportions of NSG1/2 puncta found in EEA1$^+$ early endosomal, Rab11$^+$
587 recycling endosomes, and Lamp1$^+$ lysosomes (Yap et al., 2017). Most intriguingly, this analysis
588 accounted for nearly all NSG1$^+$ punctae, but less than 80% of NSG2$^+$ punctae. Thus, it remains
589 to be determined whether there is an additional pool of unique, NSG2-containing vesicles.
590 Evidence for divergent trafficking mechanisms stems from the fact that NSG1 was previously
591 shown to be involved in a unique transcytosis mechanism for trafficking and sorting neuronal
592 L1/NgCAM to axons (Yap et al., 2008). More recently, Shi et al have shown that NSG3 associates
593 with motor proteins to coordinates dynamic microtubule dependent trafficking of LysoTracker$^+$ late
594 endosome and lysosome related organelles within axons (Shi et al., 2018). Further evidence for
595 NSG2's unique functions can be inferred by sequence homology and known NSG family protein-
596 protein interactions. NSG1 has been shown to bind to L1/NgCAM, Stx13, GRIP1, and APP
597 (Steiner et al., 2005a; Yap et al., 2008; Norstrom et al., 2010), while NSG3 binds clathrin light
598 chain (CLC), the AP1-3 adaptors, and PSD-95 (Xiao et al., 2006; Ha et al., 2012; Muthusamy et
599 al., 2012). Due to the relatively low sequence homology between NSG family members
600 (Muthusamy et al., 2009), it is likely that NSG2 has unique binding partners that can inform the
601 non-overlapping functions of NSG2 and other NSG family members with respect to
602 spatiotemporal divergence in their post-Golgi trafficking.

603 NSG2 was originally proposed to have a role in secretory trafficking for the following reasons:
604 1) it is a single-pass transmembrane protein enriched in the Golgi Apparatus and post-Golgi
605 vesicular compartments, 2) its presence in the P3 subcellular fraction of whole brain
606 ultracentrifugation and, 3) it contains a secretogranin III-like domain in its carboxy-terminus
607 (Saberan-Djoneidi et al., 1995). Recent evidence from Yap and colleagues confirmed the
608 secretory capacity of NSG2. Blocking endocytosis using a dominant negative Rab5 resulted in
609 accumulation of NSG2 on the surface of hippocampal neurons (Yap et al., 2017). Here, we found
610 that surface GluA2 levels and consequently AMPAR mEPSC amplitude were significantly
611 increased upon NSG2 overexpression, suggestive of a link between its role in the secretory

612 pathway and surface AMPAR levels. It is especially intriguing that NSG2 has an asymmetric
613 synaptic distribution, being present in approximately forty percent of excitatory synapses. As
614 mentioned, data from this and previous studies show that inhibiting either NSG1 or NSG2
615 significantly, but not completely, inhibits synaptic transmission. Thus, it will be critical to determine
616 whether other NSG family members occupy the same, or divergent populations of synapses, and
617 whether the effects of their inhibition are additive. Furthermore, understanding their temporal or
618 activity-dependence will be critical. For instance, do NSG family members mark specific subsets
619 of synapses, or do NSG proteins transiently visit most or all synapses during development or
620 during particular types of activity? Future investigations to answer these questions should reveal
621 previously unappreciated functional differences between individual excitatory synapses across
622 multiple brain regions.
623

624 **References**

625 Alberi S, Boda B, Steiner P, Nikonenko I, Hirling H, Muller D (2005a) The endosomal protein NEEP21
626 regulates AMPA receptor-mediated synaptic transmission and plasticity in the hippocampus. Molecular
627 and cellular neurosciences 29:313-319.
628 Alberi S, Boda B, Steiner P, Nikonenko I, Hirling H, Muller D (2005b) The endosomal protein NEEP21
629 regulates AMPA receptor-mediated synaptic transmission and plasticity in the hippocampus. Molecular
630 and Cellular Neuroscience 29:313-319.
631 Barford K, Yap CC, Dwyer ND, Winckler B (2017) The related neuronal endosomal proteins NEEP21 (Nsg1)
632 and P19 (Nsg2) have divergent expression profiles in vivo. The Journal of comparative neurology
633 525:1861-1878.
634 Davidson HT, Xiao J, Dai R, Bergson C (2009a) Calcyon is necessary for activity-dependent AMPA receptor
635 internalization and LTD in CA1 neurons of hippocampus. European Journal of Neuroscience 29:42-54.

636 Davidson HT, Xiao J, Dai R, Bergson C (2009b) Calcyon is necessary for activity-dependent AMPA receptor
637 internalization and LTD in CA1 neurons of hippocampus. The European journal of neuroscience 29:42-54.
638 Dittgen T, Nimmerjahn A, Komai S, Licznerski P, Waters J, Margrie TW, Helmchen F, Denk W, Brecht M,
639 Osten P (2004) Lentivirus-based genetic manipulations of cortical neurons and their optical and
640 electrophysiological monitoring in vivo. Proceedings of the National Academy of Sciences of the United
641 States of America 101:18206-18211.
642 Esteves da Silva M, Adrian M, Schatzle P, Lipka J, Watanabe T, Cho S, Futai K, Wierenga CJ, Kapitein LC,
643 Hoogenraad CC (2015) Positioning of AMPA Receptor-Containing Endosomes Regulates Synapse
644 Architecture. Cell reports 13:933-943.
645 Grabrucker A, Vaida B, Bockmann J, Boeckers TM (2009) Synaptogenesis of hippocampal neurons in
646 primary cell culture. Cell and tissue research 338:333.
647 Ha CM, Park D, Han JK, Jang JI, Park JY, Hwang EM, Seok H, Chang S (2012) Calcyon forms a novel ternary
648 complex with dopamine D1 receptor through PSD-95 protein and plays a role in dopamine receptor
649 internalization. The Journal of biological chemistry 287:31813-31822.
650 Heckl D, Kowalczyk MS, Yudovich D, Belizaire R, Puram RV, McConkey ME, Thielke A, Aster JC, Regev A,
651 Ebert BL (2014) Generation of mouse models of myeloid malignancy with combinatorial genetic lesions
652 using CRISPR-Cas9 genome editing. Nature biotechnology 32:941-946.
653 Johnson MA, Weick JP, Pearce RA, Zhang S-C (2007) Functional neural development from human
654 embryonic stem cells: accelerated synaptic activity via astrocyte coculture. Journal of Neuroscience
655 27:3069-3077.
656 Kang HJ, Kawasawa YI, Cheng F, Zhu Y, Xu X, Li M, Sousa AM, Pletikos M, Meyer KA, Sedmak G (2011)
657 Spatio-temporal transcriptome of the human brain. Nature 478:483-489.
658 Kim J, Lee S, Park K, Hong I, Song B, Son G, Park H, Kim WR, Park E, Choe HK (2007) Amygdala
659 depotentiation and fear extinction. Proceedings of the National Academy of Sciences 104:20955-20960.

660 Kruusmägi M, Zelenin S, Brismar H, Scott L (2007) Intracellular dynamics of calcyon, a neuron-specific
661 vesicular protein. Neuroreport 18:1547-1551.
662 Lasiecka ZM, Yap CC, Katz J, Winckler B (2014) Maturational conversion of dendritic early endosomes and
663 their roles in L1-mediated axon growth. The Journal of neuroscience : the official journal of the Society for
664 Neuroscience 34:14633-14643.
665 Levy JM, Chen X, Reese TS, Nicoll RA (2015) Synaptic consolidation normalizes AMPAR quantal size
666 following MAGUK loss. Neuron 87:534-548.
667 Miller JA, Ding S-L, Sunkin SM, Smith KA, Ng L, Szafer A, Ebbert A, Riley ZL, Royall JJ, Aiona K (2014)
668 Transcriptional landscape of the prenatal human brain. Nature 508:199-206.
669 Murillo JR, Goto-Silva L, Sánchez A, Nogueira FC, Domont GB, Junqueira M (2017a) Quantitative proteomic
670 analysis identifies proteins and pathways related to neuronal development in differentiated SH-SY5Y
671 neuroblastoma cells. EuPA Open Proteomics 16:1-11.
672 Murillo JR,

673 Goto-Silva, Livia, Sanchez A, Nogueira F, Domont GB, Junqueria M (2017b) Quantitative proteomic analysis
674 identifies proteins and pathways related to neuronal development in differentiated SH-SY5y
675 neuroblastoma cells. EuPA Open Proteomics 16:1-11.
676 Muthusamy N, Faundez V, Bergson C (2012) Calcyon, a mammalian specific NEEP21 family member,
677 interacts with adaptor protein complex 3 (AP-3) and regulates targeting of AP-3 cargoes. Journal of
678 neurochemistry 123:60-72.
679 Muthusamy N, Chen YJ, Yin DM, Mei L, Bergson C (2015) Complementary roles of the neuron-enriched
680 endosomal proteins NEEP21 and calcyon in neuronal vesicle trafficking. Journal of neurochemistry 132:20-
681 31.

682 Muthusamy N, Ahmed SA, Rana BK, Navarre S, Kozlowski DJ, Liberles DA, Bergson C (2009) Phylogenetic
683 analysis of the NEEP21/calcyon/P19 family of endocytic proteins: evidence for functional evolution in the
684 vertebrate CNS. Journal of molecular evolution 69:319-332.
685 Myers KM, Ressler KJ, Davis M (2006) Different mechanisms of fear extinction dependent on length of
686 time since fear acquisition. Learning & memory 13:216-223.
687 Norstrom EM, Zhang C, Tanzi R, Sisodia SS (2010) Identification of NEEP21 as a ss-amyloid precursor
688 protein-interacting protein in vivo that modulates amyloidogenic processing in vitro. The Journal of
689 neuroscience : the official journal of the Society for Neuroscience 30:15677-15685.
690 Saberan-Djoneidi D, Marey-Semper I, Picart R, Studler JM, Tougard C, Glowinski J, Levi-Strauss M (1995)
691 A 19-kDa protein belonging to a new family is expressed in the Golgi apparatus of neural cells. The Journal
692 of biological chemistry 270:1888-1893.
693 Schwenk J, Baehrens D, Haupt A, Bildl W, Boudkkazi S, Roeper J, Fakler B, Schulte U (2014) Regional
694 diversity and developmental dynamics of the AMPA-receptor proteome in the mammalian brain. Neuron
695 84:41-54.
696 Sharma K, Fong DK, Craig AM (2006) Postsynaptic protein mobility in dendritic spines: long-term
697 regulation by synaptic NMDA receptor activation. Molecular and Cellular Neuroscience 31:702-712.
698 Shi L, Hines T, Bergson C, Smith D (2018) Coupling of microtubule motors with AP-3 generated organelles
699 in axons by NEEP21 family member calcyon. Molecular biology of the cell 29:2055-2068.
700 Steiner P, Sarria J-CF, Glauser L, Magnin S, Catsicas S, Hirling H (2002) Modulation of receptor cycling by
701 neuron-enriched endosomal protein of 21 kD. The Journal of cell biology 157:1197-1209.
702 Steiner P, Alberi S, Kulangara K, Yersin A, Sarria JCF, Regulier E, Kasas S, Dietler G, Muller D, Catsicas S
703 (2005a) Interactions between NEEP21, GRIP1 and GluR2 regulate sorting and recycling of the glutamate
704 receptor subunit GluR2. The EMBO journal 24:2873-2884.

705 Steiner P, Alberi S, Kulangara K, Yersin A, Sarria JC, Regulier E, Kasas S, Dietler G, Muller D, Catsicas S,
706 Hirling H (2005b) Interactions between NEEP21, GRIP1 and GluR2 regulate sorting and recycling of the
707 glutamate receptor subunit GluR2. The EMBO journal 24:2873-2884.
708 Utvik J, Haglerød C, Mylonakou M, Holen T, Kropf M, Hirling H, Skare Ø, Laake P, Ottersen O, Haug F-M
709 (2009) Neuronal enriched endosomal protein of 21 kDa colocalizes with glutamate receptor subunit
710 GLUR2/3 at the postsynaptic membrane. Neuroscience 158:96-104.
711 Vazdarjanova A, Bunting K, Muthusamy N, Bergson C (2011) Calcyon upregulation in adolescence impairs
712 response inhibition and working memory in adulthood. Molecular psychiatry 16:672-684.
713 Weick JP, Held DL, Bonadurer GF, 3rd, Doers ME, Liu Y, Maguire C, Clark A, Knackert JA, Molinarolo K,
714 Musser M, Yao L, Yin Y, Lu J, Zhang X, Zhang SC, Bhattacharyya A (2013) Deficits in human trisomy 21 iPSCs
715 and neurons. Proceedings of the National Academy of Sciences of the United States of America 110:9962-
716 9967.
717 Xiao J, Dai R, Negyessy L, Bergson C (2006) Calcyon, a novel partner of clathrin light chain, stimulates
718 clathrin-mediated endocytosis. Journal of Biological Chemistry 281:15182-15193.
719 Yap CC, Winckler B (2012) Harnessing the power of the endosome to regulate neural development.
720 Neuron 74:440-451.
721 Yap CC, Digilio L, McMahon L, Winckler B (2017) The endosomal neuronal proteins Nsg1/NEEP21 and
722 Nsg2/P19 are itinerant, not resident proteins of dendritic endosomes. Scientific reports 7:10481.
723 Yap CC, Wisco D, Kujala P, Lasiecka ZM, Cannon JT, Chang MC, Hirling H, Klumperman J, Winckler B (2008)
724 The somatodendritic endosomal regulator NEEP21 facilitates axonal targeting of L1/NgCAM. The Journal
725 of cell biology 180:827-842.

726

727

728 **Figure legends**

729 **Figure 1 (Also Figure 1-1, 1-2 and 1-3). A subset of NSG2 punctae localize to postsynaptic**
730 **densities of excitatory synapses.** (A) Representative confocal images of primary hippocampal
731 neurons (DIV4) illustrate a perinuclear as well as punctate NSG2 expression pattern (magenta;
732 arrows) in β_{III}-Tubulin$^+$ neurons (blue). No NSG2 expression was observed in GFAP$^+$ astrocytes
733 (cyan; arrowheads). The punctate expression pattern of NSG2 was found in all neurons tested
734 up to DIV30 (Figure 1-1). (B) magnified image of yellow box in the Merge panel of A. (C)
735 Immunofluorescent images illustrate NSG2 (magenta; arrows) punctae exclusively in MAP2$^+$
736 (blue) dendrites and absence of NSG2 punctae in SMI312$^+$ axons (cyan; arrowheads) at DIV14.
737 (D) magnified image of yellow box in the Merge panel of C. (E) Representative western blot
738 image demonstrating the specificity of the NSG2 antibody in detecting NSG2 (NSG2-mC; top
739 panel, ~48kDa band; middle lane) but not the closely-related protein NSG1 (NSG1-GFP; top
740 panel, ~48kDa). Bottom panel shows the β-actin loading control. (F) Representative western
741 blot image demonstrating the expression profile of the NSG2 from mouse whole brain lysate
742 during development (top panel, ~19kDa band). While GAPDH was used as a loading control
743 (middle panel) it shows variability across development. The blot was also stained with
744 Coomassie (bottom panel) to demonstrate equal protein loading. (G) Confocal images showing
745 endogenous NSG2 (left panels) and overexpressed NSG2-mC (right panels) colocalized with
746 HOMER1$^+$ punctae (arrowheads; HOMER1 panel and Merge). Endogenous NSG2 and NSG2-
747 mC were frequently found adjacent to Synapsin1$^+$ punctae (e.g. leftmost arrowheads). Individual
748 panels for HOMER1$^+$ (white) and SYN1$^+$ (cyan) are shown for clarity. The colocalization profile
749 of NSG2 or NSG2-mC (magenta trace) with HOMER1 (white trace) for the indicated punctae
750 are indicated in the bottom panels. Some NSG2 punctae were not found colocalized to either
751 HOMER1 or SYN1 punctae (arrow). (H) Quantification of colocalization of Homer1 with either
752 endogenous NSG2 or NSG2-mC. Bars represent mean ± S.E.M for n=10 for each group;

753 *p=0.024. Scale bar represents 10μm (A-B), 2 μm (B, D and G; left panels) or 4 μm (G; right
754 panels).
755
756 **Figure 2 (Also Figure 2-1). NSG2 colocalizes with AMPAR subunits GluA1 and GluA2.** (A-
757 B) Representative confocal images of primary hippocampal neurons at DIV15 showing
758 perinuclear and punctate NSG2 (magenta) in $MAP2^+$ (blue) neurites along with surface
759 expressed GluA1 punctae (A, cyan), and GluA2 punctae (B, cyan). Separated color panels for
760 individual markers from the boxed regions have been magnified for clarity (right panels). Lower
761 right panels in A-B show the colocalization profile for NSG2 (magenta)/GluA1 (cyan, panel A)
762 and NSG2 (magenta)/GluA2 (cyan, panel B) across the indicated punctae (arrowheads). (C-D)
763 Quantification of colocalization for NSG2 with surface GluA1 punctae (6423 NSG2 and 5392
764 GluA1 puncta from 10 neurons) and NSG2 with surface GluA2 punctae (6874 NSG2 and 5963
765 GluA2 puncta from 9 neurons) respectively from 3 independent cultures. Scale bars represent
766 10μm (A, B; left panels) and 2 μm (A, B; right panels).
767
768 **Figure 3 (Also Figure 3-1). NSG2 interacts with AMPAR subunits GluA1 and GluA2.** (A)
769 Co-Immunoprecipication (Co-IP) of overexpressed, fluorophore-conjugated proteins.
770 Representative digitized western blots from the automated western blot system (see methods)
771 showing that using the anti-RFP antibody to pull down NSG2-mC (IP: RFP, arrow) could Co-IP
772 both YFP-GluA1 and GFP-GluA2 (IP: mCherry, arrowhead). A control IgG antibody did not IP
773 nor detect any target proteins (IP: IgG); the heavy chain of mouse and anti-RFP was detected
774 by the anti-mouse secondary antibody used to detect mouse anti-GluA1/2. NSG2-mC (arrow),
775 YFP-GluA1 and GFP-GluA2 (arrowhead) were detected in the input (Input). Traditional western
776 blotting techniques were performed to confirm that GluA2 co-immunoprecipitates with NSG2-
777 mC (Figure 3-1). Samples were taken from HEK293T cells co-expressing NSG2-mC and either

YFP-GluA1 or GFP-GluA2. (B) Immunoprecipitation of overexpressed, unlabeled NSG2 with fluorophore-conjugated proteins with antibodies directed toward endogenous protein epitopes. Anti-GluA1 and Anti-GluA2 antibodies immunoprecipitated YFP-GluA1 and GFP-GluA2 respectively (IP: GluA1 and IP: GluA2, arrowhead). Unlabeled NSG2 (arrow) coexpressed in HEK293T cells was also detected using these same conditions, confirming the Co-IP; control IgG did not IP nor detect any target proteins (IP: IgG). NSG2, YFP-GluA1 and GFP-GluA2 are detected in the input (Input; GluA1; GluA2, arrowhead; NSG2, arrow). Lower bands in NSG2 lanes of control IgG pull down conditions is thought to be non-specific is found in all similar reaction conditions and migrates faster than NSG2. (C) Immunoprecipitation from *in vivo* samples (whole brain lysate of P0 mouse). Anti-GluA1 and Anti-GluA2 antibodies immunoprecipitated endogenous GluA1 and GluA2 (IP: GluA1 and IP: GluA2, arrowhead) as well as endogenous NSG2 (arrow). All target proteins were detected in the input lanes (Input; GluA1 and GluA2, arrowhead; NSG2, arrow). Control mouse IgG antibody did not pull down GluA1, GluA2, or NSG2 (IP: IgG). As expected, heavy chain and light chains from antibodies used for pull down were detected in most Co-IP conditions (all “IP” lanes).

Figure 4 (Also Figure 4-1, 4-2 and 4-3). Knockout of NSG2 decreases mEPSC frequency. (A) Representative confocal images of primary hippocampal neurons at DIV15 showing robust NSG2 (Magenta) in MAP2^{+} (blue) neurons transduced with control CRISPR GFP lentivirus (cyan; top panels) whereas neurons transduced with CRISPR KO NSG2 lentivirus (cyan, bottom panels) show the absence of NSG2 (arrow; bottom panels); NSG2 (magenta) is present in an adjacent neuron not transduced with the CRISPR KO NSG2 lentivirus in the same field (arrowhead; bottom panels). (B) Representative traces from whole cell patch clamp recordings from neurons expressing either control CRISPR GFP (upper trace, black) or CRISPR KO NSG2 (bottom trace, green). Averaged mEPSCs from both control (black, n=10) and NSG2 KO (green, n=13) are shown to the right. (C) Pooled data revealed a significant decrease in mEPSC

804 frequency in neurons expressing NSG2 KO compared to cells expressing control CRISPR GFP
805 (**p = 0.001). The amplitude of mEPSCs was not significantly different between groups (p =
806 0.34). Data in the KO group were derived only from neurons devoid of NSG2 confirmed by post-
807 recording immunostaining of Lucifer yellow injected neurons (Figure 4-1). NSG2 KO did not alter
808 outward potassium I/V relationship (Figure 4-2). (D) Quantification of presynaptic marker
809 Synapsin1^{+} punctae (control, n=10; NSG2 KO, n=10; p = 0.46) and post synaptic marker
810 PSD95^{+} punctae (control, n=9; NSG2 KO, n=11; p = 0.18). (E) Representative confocal images
811 illustrate PSD95 immunofluorescence (cyan) in neurons expressing CRISPR KO NSG2 (right
812 panels) or controls CRISPR GFP (left panels). GFP expression from both groups (top panels) is
813 presented in grayscale for clarity. Quantification revealed a significant reduction in PSD95
814 fluorescence intensity in neurons expressing NSG2 KO (n=11) compared to controls (n=9; *p =
815 0.029). (F) Pooled data show that the number of surface GluA1^{+} punctae (left; control, n=10 and
816 NSG2 KO, n=9; p = 0.86) and surface GluA2^{+} punctae (right; Control, n=10 and NSG2 KO, n=9;
817 p = 0.18) remained unchanged between groups. Bars represent mean ± S.E.M. Scale bars
818 represent 10μm in (A) and 1 μm (E).
819
820 **Figure 5. Overexpression of NSG2 increases mEPSC amplitude.** (A) Representative traces
821 from whole cell patch clamp recordings from neurons expressing either mCherry alone (upper
822 trace, black) or NSG2-mC (bottom trace, red). Averaged mEPSCs from both control (black, n=11)
823 and NSG2-mC (red, n=10) are shown to the right. (B) Pooled data illustrate that neurons
824 expressing NSG2-mC showed a significant increase in mEPSC amplitude compared to controls
825 (**p = 0.01) whereas the frequency of mEPSCs was not different between groups (p = 0.35). (C)
826 Neither GluA1^{+} punctae number (p = 0.58) nor Relative Fluorescence Intensity (p = 0.36) were
827 significantly different between groups (mCherry vs NSG2-mC). (D) Representative confocal
828 images showing neurons expressing either mCherry alone (left panels) or NSG2-mC (right
829 panels) stained for MAP2 (magenta) and surface GluA2 (cyan). Individual GluA2 and MAP2

expression from both groups (top two panels) are presented in grayscale for clarity. (E) Pooled data revealed the number of GluA2^{+} punctae was significantly increased in neurons expressing NSG2-mC (n=10) compared to controls (n=10; *p = 0.02) while Relative Fluorescence Intensity remained unchanged (p = 0.19). Bars represent mean ± S.E.M; A.U. = Arbitrary units. Scale bars represent 2 μm.

Extended Data Figure Legends

Figure 1-1 (Supports Figure 1). NSG2 is robustly expressed in human pluripotent stem cell-derived neurons (hPSNs). (A) Representative confocal immunofluorescence images of Day30 hPSNs showing the expression and distribution of NSG2 (magenta; arrows) in β_{III}-Tubulin^{+} neurons (cyan). DAPI^{+} nuclei are indicated in white. (B) Representative confocal images of Day50 hPSNs showing the expression and distribution of NSG2 (magenta; arrows) in β_{III}-Tubulin^{+} neurons (cyan). DAPI^{+} nuclei are indicated in white. (C) Representative confocal images of hPSNs illustrate NSG2 (magenta; arrows) expression restricted to MAP2^{+} (blue) neurons and absent from Pax6^{+} neural progenitors in Day30 hPSN cultures. Nuclear Pax6^{+} (cyan; arrowheads) colocalized with DAPI^{+} nuclei (white; arrowheads). Scale bars represent 10μm.

Figure 1-2 (Supports Figure 1). NSG2 remains expressed in mouse hippocampal neurons at DIV30. Representative confocal immunofluorescence images of primary hippocampal neurons (DIV30) showing the expression and distribution of NSG2 (magenta; arrow) in β_{III}-Tubulin^{+} neurons (cyan). DAPI^{+} nuclei are indicated in white. Scale bars represent 5μm.

Figure 1-3 (Supports Figure 1). NSG2 expression in hPSNs is neuron-specific and somatodendritic. (A) Representative confocal images of hPSNs illustrate NSG2 expression is perinuclear (magenta; arrows) and localized to punctae distributed in MAP2^{+} (blue) dendrites;

855 NSG2 punctae are absent in GFAP$^+$ astrocytic processes (cyan; arrowheads) at Day50. Far right
856 panel shows magnified image of yellow box in 'Merge'. (B) Representative confocal images of
857 hPSNs illustrate NSG2 punctae (magenta; arrows) exclusively in MAP2$^+$ (blue) dendrites but
858 absent from SMI312$^+$ axons (cyan; arrowheads) at Day50. Far right panel shows magnified image
859 of yellow box in 'Merge'. DAPI$^+$ nuclei are indicated in white. Scale bars represent 10μm.
860
861 **Figure 2-1 (Supports Figure 2). NSG2 colocalizes with AMPAR subunits GluA1 in hPSNs.**
862 Representative confocal images of hPSNs at Day50 overexpressing NSG2-mC showing
863 perinuclear and punctate NSG2 (magenta) in MAP2$^+$ (blue) dendrites along with surface
864 expressed GluA1 punctae (cyan). Separate magnified panels for each marker indicated by the
865 boxed region are provided for clarity (right panels). Colocalized NSG2 punctae (magenta) and
866 surface GluA1 (cyan) are indicated by arrows while non-colocalized proteins are indicated by
867 arrowheads. Scale bars represent 10μm (left panel) and 2 μm (right panels).
868
869 **Figure 3-1 (Supports Figure 3). NSG2 and GluA2 physically interact.** Representative western
870 blot image showing Co-IP of NSG2-mC and GluA2 by anti-RFP in lysates from HEK293T cells
871 co-expressing both proteins (Co-IP RFP Trap; NSG2-mC, red bands; GFP-GluA2, green bands).
872 The specificity of antibodies is confirmed by the absence of bands in lysates from untransfected
873 cells (Untransfected) and presence of bands of expected size in the input lane (Input-
874 coexpression lysate). Anti-RFP was unable to Co-IP NSG2-mC GluA2 when the two proteins
875 were overexpressed in different HEK293T cultures, and lysates were incubated together and then
876 subject to immunoprecipitation (*In vitro* incubation).
877
878 **Figure 4-1 (Supports Figure 4). Lucifer Yellow injections used to verify NSG2 KO in**
879 **recorded neurons.** Representative confocal images of primary hippocampal neurons (DIV15)
880 showing the absence of NSG2 (magenta, arrow) in MAP2$^+$ neurons (blue) transduced with

881 CRISPR KO-NSG2 lentivirus (cyan). Lucifer Yellow was injected into neurons expressing
882 CRISPR KO-NSG2 during whole cell patch clamp experiments (Inset: Luc. Yellow; Figure 4).
883 NSG2 (magenta) was present in MAP2$^+$ neurons not expressing CRISPR KO-NSG2
884 (arrowhead). Scale bars represent 10μm.
885
886 **Figure 4-2 (Supports Figure 4). Alterations in NSG2 levels does not affect voltage-gated**
887 **potassium currents.** (A-B) Current-voltage relationship plots illustrating that neither NSG2-KO
888 (A, open circles) nor NSG2-mC overexpression (B, open circles) caused a significant change to
889 transient potassium current elicited by voltage steps compared to controls (A-B, black squares).
890 (C-D) Representative traces from plots in panels A-B in response to voltage steps from -50mV
891 to +50mV (step size, 10mV).
892
893 **Figure 4-3 (Supports Figure 4). Knockout of NSG2 does not alter NSG1 levels.** (A)
894 Representative confocal images of primary hippocampal neurons (DIV15) showing the presence
895 of NSG1 (white, arrowhead) in MAP2$^+$ (blue) neurons from GFP$^+$ cells transduced with either
896 CRISPR control (cyan; top panels) or CRISPR KO-NSG2 lentivirus (cyan; bottom panels).
897 Middle panels illustrate the presence of NSG2 (magenta, arrow) in MAP2$^+$ neurons (blue)
898 transduced with CRISPR control (top panels) and absence of NSG2 (arrow) in MAP2$^+$ neurons
899 (blue) transduced with CRISPR KO-NSG2 lentivirus (cyan). Scale bars represent 10μm. (B)
900 Pooled data show that the density of NSG1 punctae remained unchanged between groups
901 (Bars represent mean ± S.E.M, n=10 per group; p = 0.97). (C) Representative agarose gel
902 showing digested fragments from mouse NSG2 DNA amplicon (arrow) were observed in cells
903 that received either gRNA#1 or gRNA#2 + T7, but not in control or without T7.

Figure 1

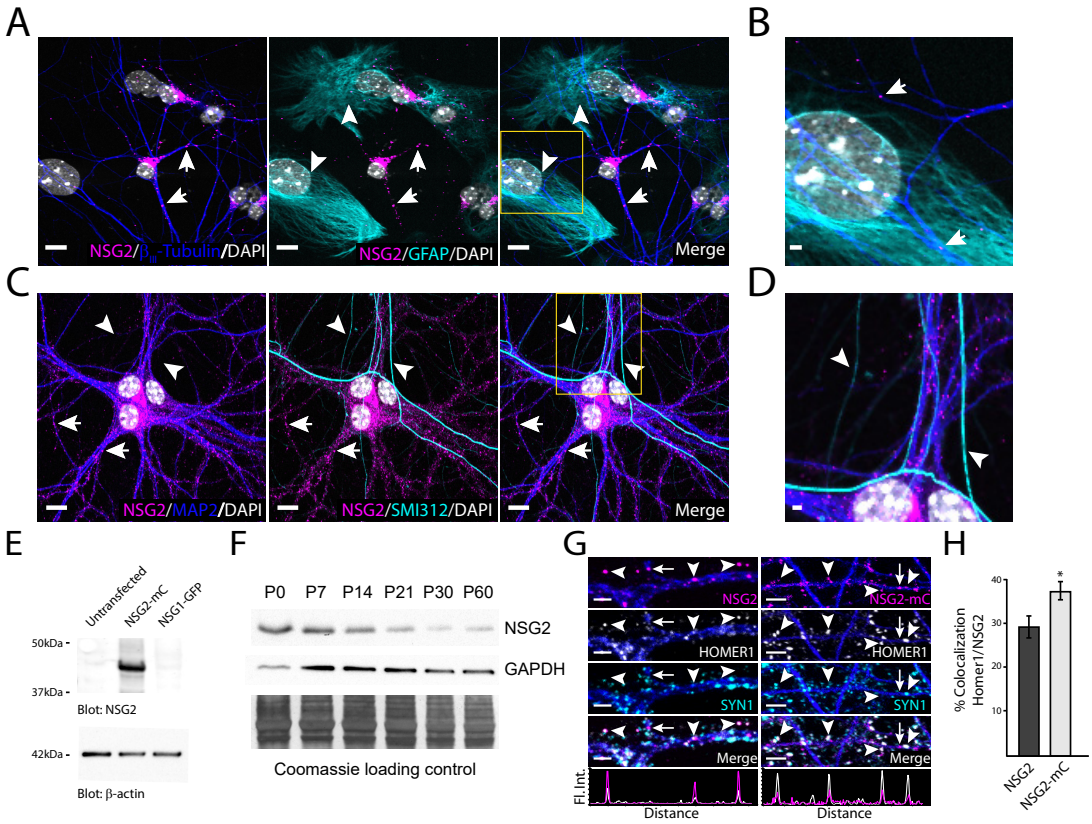

Figure 2

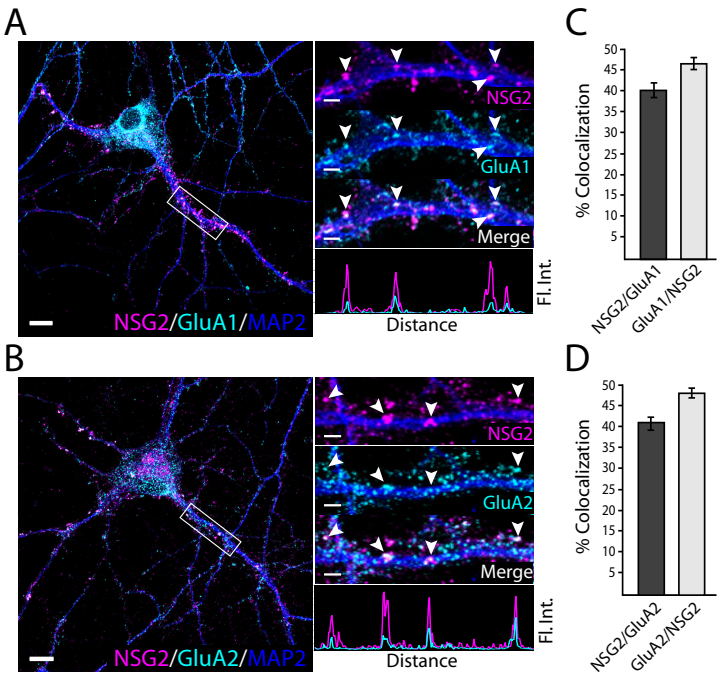

Figure 3

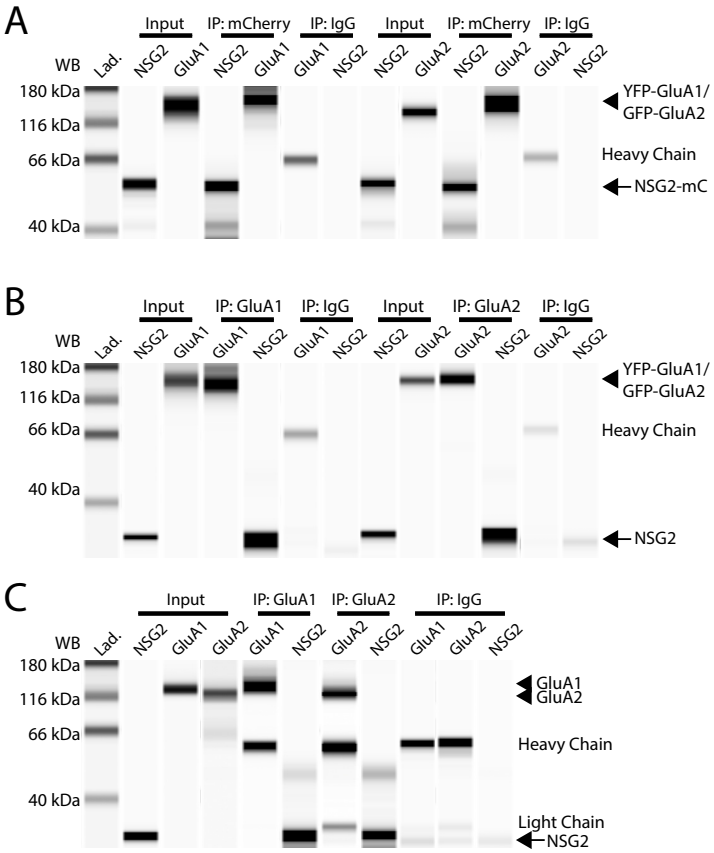

Figure 4

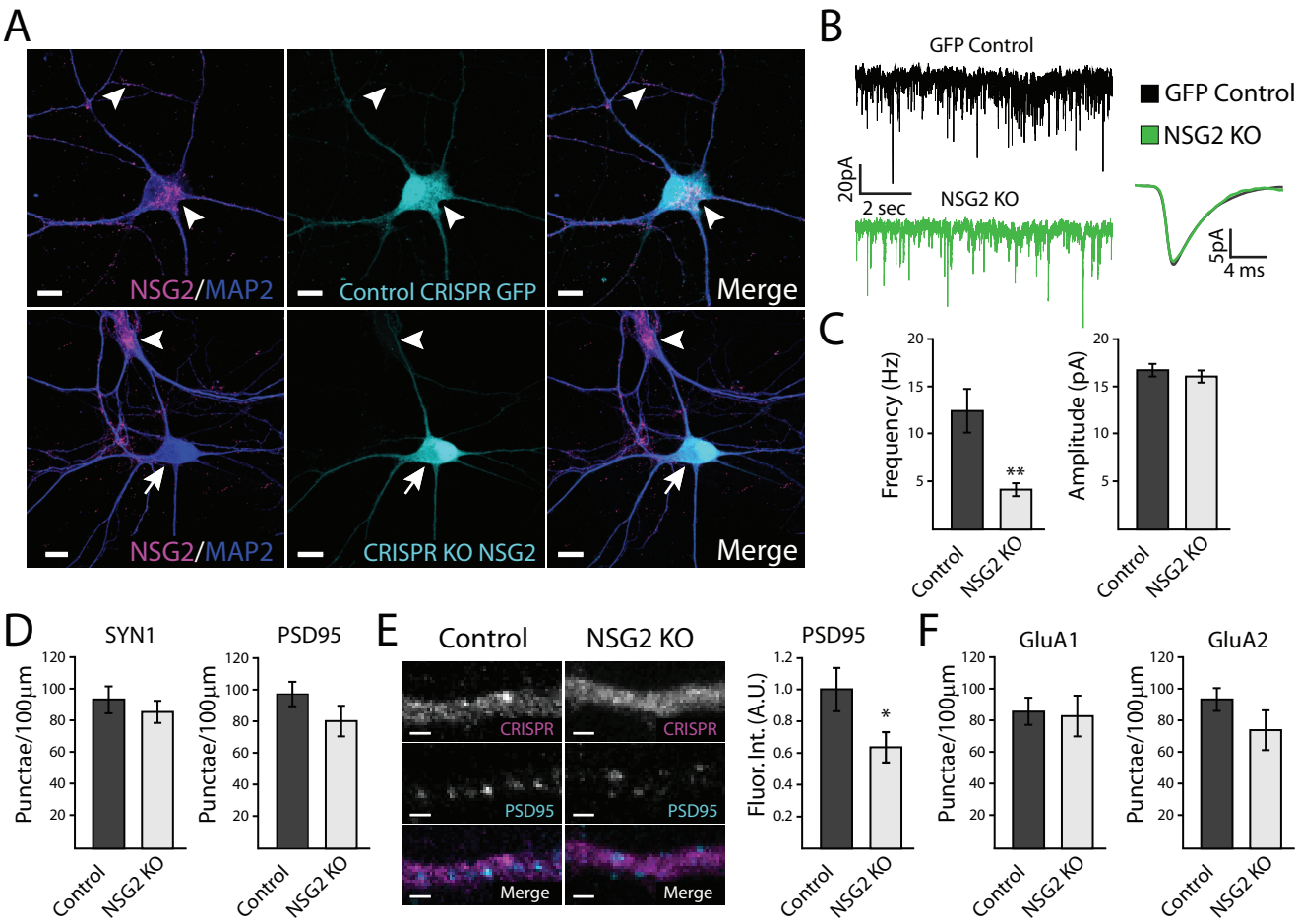

Figure 5